

Cross-Domain 3D Equivariant Image Embeddings

Carlos Esteves^{1,2*}, Avneesh Sud², Zhengyi Luo¹, Kostas Daniilidis¹, Ameet Makadia²

¹GRASP Laboratory, University of Pennsylvania ²Google AI

{machc,zhengyi,kostas}@seas.upenn.edu {avneesh,makadia}@google.com

November 19, 2021

Abstract

Spherical convolutional networks have been introduced recently as tools to learn powerful feature representations of 3D shapes. Spherical CNNs are equivariant to 3D rotations making them ideally suited for applications where 3D data may be observed in arbitrary orientations. In this paper we learn 2D image embeddings with a similar equivariant structure: embedding the image of a 3D object should commute with rotations of the object. We introduce a cross-domain embedding from 2D images into a spherical CNN latent space. Our model is supervised only by target embeddings obtained from a spherical CNN pre-trained for 3D shape classification. The trained model learns to encode images with 3D shape properties and is equivariant to 3D rotations of the observed object. We show that learning only a rich embedding for images with appropriate geometric structure is in and of itself sufficient for tackling numerous applications. Evidence from two different applications, relative pose estimation and novel view synthesis, demonstrates that equivariant embeddings are sufficient for both applications without requiring any task-specific supervised training.

1 Introduction

The recent success of deep convolutional neural networks in computer vision has shown that large training datasets and task-specific supervision are suffi-

cient to learn rich feature representations that may generalize across tasks [12]. However, there is growing body of evidence that suggests strong priors in the models are necessary when facing limited training data or supervision, and in particular strong geometric priors on latent representations have been useful as geometric supervision is not easily available at scale (e.g. [26, 47, 43]).

A desirable property for an image embedding is robustness to 3D geometric transformations of the scene. 3D rotations, in particular, are a nuisance to computer vision algorithms because even small rotations of 3D objects in the world can induce large transformations in image space. In recent years there has been much attention given to the study of equivariant neural networks (e.g. [38]), as equivariant maps provide a natural formulation to address group transformations on images. Despite these advances, designing a 3D rotation equivariant map of 2D images is an open challenge. This is because the rotation of a 3D object does not act directly on the pixels of the resulting image due to the camera projection. Thus, an equivariant map cannot be constructed by design and instead an (approximate) equivariant map must be learned. This is the central task of the paper: *how can we learn an embedding for 2D images of 3D objects that is equivariant to 3D rotations of the object?*

Our proposal is inspired by recent works on 3D rotation equivariant CNNs for 3D shape representations [3, 6]. These works show that spherical convolutional networks can achieve state of the art performance on 3D shape classification and pose estimation tasks, and these networks’ equivariance prop-

* This work was done during an internship at Google.

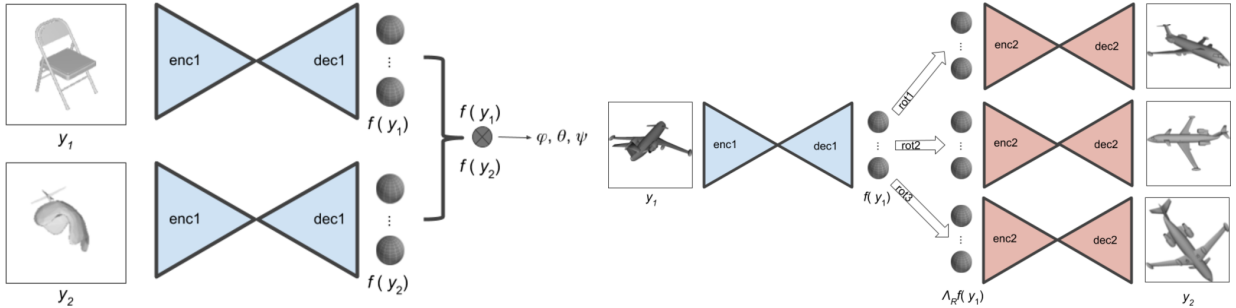


Figure 1: **Overview.** We learn category based spherical 3D equivariant embeddings that can be correlated for relative pose estimation, and rotated for novel view synthesis. *Left: relative pose estimation.* Given 2 images of objects from same class, we obtain the respective spherical embeddings. The relative pose is computed from the spherical correlation between the spherical embeddings. *Right: novel view synthesis.* We first embed the input view into the spherical representation, then we apply the target rotation to the spherical feature maps, and feed them to the synthesizer to generate novel views.

erties mean their performance does not suffer when considering 3D shapes in arbitrary orientations.

In this work we propose to learn an equivariant embedding of an image by mapping it into the equivariant feature space of a spherical CNN trained on datasets of 3D shapes. Our approach is unique in that we are directly supervising the desired target embeddings and we do not consider any other task-specific training losses. By bootstrapping with features of 3D shapes, our trained model maps images to features that (1) encode the shape properties of the observed 3D object and (2) have an underlying spherical structure that is equivariant to rotations of the 3D object.

We show that the learned feature representations are themselves often sufficient for applications without requiring any additional task-specific supervised training. We illustrate this point by showing results on two very different challenges:

Relative orientation estimation Our model maps 2D images to feature maps defined on the sphere (Fig. 1-left). Due to the rotation equivariance of these feature maps, we can recover the relative orientation between two embeddings by finding the rotation that brings them into alignment (we do this simply with spherical cross-correlation with-

out running any regression as an unsupervised spatial transformer [14] would do). We show this method approaches state of the art performance even though it requires no task-specific training.

Novel view synthesis The learned image embeddings also encode the necessary shape properties to synthesize new views. By simply training an image decoder from the spherical embedding space using an image autoencoder loss, we have a model for novel view synthesis. New views are generated by simply rotating the latent embedding (Fig. 1-right). Similarly to the approach for relative orientation described above, our model requires no task specific supervision.

To reiterate, our main contribution is a novel cross-domain neural model that can map 2D images into a 3D rotation equivariant feature space. We consider the relative pose and view synthesis tasks as proxies for analyzing the representation power of our learned embeddings. Nonetheless, our promising experimental results indicate our cross-domain embeddings may be useful for a variety of tasks.

In the following section we briefly cover related works before presenting the details of our method and experimental results.

2 Related work

Although there have been a number of recent works that explore geometric (either explicit or implicit) representations in the context of convolutional neural networks (see for example [45, 5]), we omit a full survey and include the works closest to ours.

The encoder-decoder in [26] maps images to explicit 3D embeddings, allowing them to be directly rotated and subsequently decoded into the corresponding image. In contrast to our approach, training examples must cover all pairs of viewpoints (sample complexity $\mathbf{SO}(3) \times \mathbf{SO}(3)$), whereas our model trains with one view at a time (sample complexity $\mathbf{SO}(3)$).

KeypointNet [33] introduces a model that learns category-specific semantic keypoints and their detectors using only a geometric loss (multiview consistency). They show that the learned keypoints are also very useful for determining relative pose. Although successful at recovering constrained motions (only a hemisphere of 2D rotations, no in-plane image rotation), the method struggles when exposed to arbitrary 3D rotations due to lack of rotation equivariance.

Falorsi *et al.* [7] introduced homeomorphic variational autoencoders, which learn a manifold-valued latent representation homeomorphic to the latent manifold of the high dimensional data. While this provides a powerful unsupervised way to learn an $\mathbf{SO}(3)$ -latent-embedding for images, it is presently unclear if it can scale to practical scenarios (requires a dense sampling of views to learn a continuous embedding, dealing with intra-class variations, etc).

Pose Estimation: The task of object pose estimation has been a long standing problem with numerous applications in computer vision and robotics. Initializing 6DoF object pose estimation with a bounding box from an object detector reduces the challenging task to 3D orientation estimation [32, 19], and 3DoF translation estimation assumes known object instance. Thus, like many related approaches we focus our experiments solely on the difficult task of relative 3D orientation estimation. Keypoint-based methods for object pose estimation include [23] and [11], the former predicting semantic keypoints and the latter bounding box corners, from which object

pose is determined from a PnP algorithm. An alternative to keypoint-based techniques are recent methods that directly estimate object pose as classification or regression. In [35] the space of viewpoints is quantized and a CNN is trained for classification, and [30] introduces a geometric-weighted classification loss for fine-grained classification. Kanezaki *et al.* [15] train a joint 3D object classification and pose CNN from multiple views with unknown viewpoints. The viewpoint sphere is sampled discretely providing limited resolution in the estimated pose. Mahendran *et al.* [19] introduces a carefully designed CNN for viewpoint regression, analyzing different representations and geodesic loss functions, and [21] introduce a MultiBin orientation regression network.

Note, in contrast to these methods, we do not propose to learn the relative pose from images directly, but rather learn geometrically-structured embeddings. We are inspired by recent approaches for learning group-equivariant representations (e.g. [38, 3, 4, 6, 17]).

Novel View Synthesis: Novel view synthesis deals with the task of creating realistic images from previously unseen viewpoints. Many techniques use an encoder-decoder architecture, and augment the latent code with pose information [34]. [44] attempts to handle large view changes using recurrent units to model incremental rotations. Other approaches use additional semantic information such as optical flow [46] and depth maps [9]. More recent approaches introduce geometric transformations on the latent space towards novel view synthesis of faces [39] and humans [26]. Select self-supervised methods learn a latent with geometric priors using differentiable rendering to match semantic maps [45], shading information [13], fusing latent from multiple views and improving synthesis using multiple rendering steps [5].

In contrast, we explore novel view synthesis under rotations as an explicit mapping from a geometric embedding to an image.

The key ingredient in our approach is a novel method to map 2D images to rotation-equivariant 3D shape embeddings, essentially encoding an image with 3D geometric structure. We note that the choice of geometric representation (spherical embeddings) is intentional in order to maintain rotation equivari-

ance. Alternative geometric representations such as volumetric (e.g. single-view volumetric reconstruction from [36]) would not be rotation equivariant.

3 Method

In this section we detail our image embedding model. We begin by revisiting spherical CNNs (Section 3.1) as a means to learn rich equivariant embeddings for 3D shapes, and Section 3.2 introduces our cross-domain architecture that learns to map 2D images into the same embedding space. Sections 3.2.3 and 3.2.4 will describe how these image embeddings can be used for relative pose estimation and novel view synthesis.

3.1 Spherical CNNs

Spherical CNNs [3, 6] produce 3D rotation equivariant feature maps for inputs defined on the sphere. In practice these methods have been useful for a variety of 3D shape analysis tasks as it is common for inputs to appear in arbitrary pose, for which equivariance is a particularly helpful property. In this work we adopt the spherical convolutional model introduced in [6] due to its efficiency and performance on 3D shape alignment tasks¹. We briefly summarize the spherical CNN below (see [6] for details). For functions x_1, x_2 defined on the sphere, their convolution product is defined as

$$(x_1 \star x_2)(p) = \int_{R \in \mathbf{SO}(3)} x_1(R\eta) x_2(R^{-1}p) dR, \quad (1)$$

where η is the north pole of the sphere (the stationary point under $\mathbf{SO}(2)$). This extends to K -channel inputs in a straightforward manner

$$(x_1 \star x_2)(p) = \sum_{k=0}^{K-1} \int_{R \in \mathbf{SO}(3)} x_{1,k}(R\eta) x_{2,k}(R^{-1}p) dR, \quad (2)$$

where $x_{\cdot,k}$ denotes the k -th channel.

¹It is important to note that we are tackling the more challenging problem of relative 3D pose from 2D images.

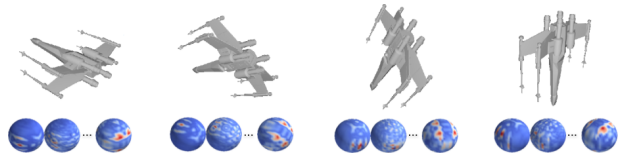


Figure 2: **Spherical CNN feature maps.** Given an input mesh (top), a spherical CNN produces a set of learned equivariant feature maps at different resolutions (bottom). Note how the feature maps follow the shape rotation.

These convolutions are the primary building blocks of spherical CNNs. We define s as a spherical CNN that maps K_{in} -channel spherical inputs to K_{out} -channel spherical feature maps. Precisely, in the single-channel case we have $s: L^2(S^2) \mapsto L^2(S^2)$ where $L^2(S^2)$ denotes square-integrability, which is necessary for the efficient evaluation of convolution in the spectral domain.

An important property of the spherical CNN is 3D rotation equivariance. For any $x: S^2 \mapsto \mathbb{R}^{K_{\text{in}}}$, we have

$$s(\Lambda_R x) = \Lambda_R s(x), \quad (3)$$

where Λ_R is the rotation operator by $R \in \mathbf{SO}(3)$ ². Technically this equivariance is only approximate as the nonlinear activations (ReLU) and spatial pooling operations break the bandlimiting assumptions which otherwise guarantee equivariance. However, in practice these errors are negligible [6].

To use spherical CNNs with 3D shapes, we must provide a map $r(M)$ which converts any 3D shape M to a spherical representation. While there are many choices for r we use the simple ray-casting technique of [6]. Most importantly, $r(M)$ is equivariant to 3D rotations which ensures end-to-end equivariance of our 3D shape feature maps: $s(r(\Lambda_R M)) = \Lambda_R s(r(M))$. Figure 2 shows sample feature maps from a spherical CNN trained for shape classification.

²We use Λ_R as a generic rotation operator that can be applied to 3D shapes and spherical functions, scalar or vector-valued. Interpretation should be clear from context.

3.2 Cross-domain spherical embeddings

In the previous section we summarized a rotation equivariant spherical CNN model for 3D shape inputs: $s(r(M))$. The primary objective of this work is to learn an *image* embedding that can capture similar underlying 3D shape properties and equivariant structure. Specifically, let us define an RGB image as the projection c of a shape M (c can be any usual camera projection model, e.g. perspective or orthographic). We seek a map $f(c(M))$ that captures the shape properties of M and retains an equivariant structure: $f(c(\Lambda_R M)) = \Lambda_R f(c(M))$. This is challenging because $c(M)$ is not 3D rotation equivariant as it is a camera projection, so we cannot have equivariance by construction. We propose to learn an approximately equivariant embedding model f using a spherical CNN for 3D shapes, i.e. a pretrained $s(r(M))$, as supervision: we wish to learn f such that $f(c(M)) = s(r(M))$. If learned successfully, the equivariance of f follows simply from (3):

$$\begin{aligned} f(c(\Lambda_R M)) &= s(r(\Lambda_R M)) \\ &= \Lambda_R s(r(M)) = \Lambda_R f(c(M)) \end{aligned} \quad (4)$$

Since $c(M)$ and $r(M)$ are fixed and not part of the trainable model, we substitute $y = c(M)$ and $x = r(M)$ going forward to simplify notation.

The two major design challenges are deciding the structure of $f(y)$ and the training loss $\mathcal{L}(x, y)$ from predicted embedding $f(y)$ to the target ground truth $s(x)$. We describe first the training loss. Since $s(x)$ (and thus also $f(y)$) produces a spherical embedding with multiple channels, for simplicity we describe the loss for a single channel (in general the loss is aggregated over the channels). The implementation of the spherical CNN represents the spherical function $s(x)$ on a grid via equirectangular projection. A discretized $s(x)$ of resolution $N \times N$ can be indexed by the pair (θ_i, ϕ_j) , $i, j \in \{0, 1, \dots, N-1\}$. The θ_i uniformly sample colatitude, and similarly ϕ_j uniformly

sample azimuth. The loss is given by

$$\mathcal{L}(x, y) = \frac{1}{N^2} \sum_{i,j=0}^{N-1} \mathcal{H}(\sin(\theta_i)(f(y) - s(x))(\theta_i, \phi_j)) \quad (5)$$

$$\mathcal{H}(\alpha) = \begin{cases} 0.5\alpha^2 & \text{for } |\alpha| \leq 1, \\ |\alpha| - 0.5 & \text{otherwise.} \end{cases} \quad (6)$$

Here a weight is introduced to account for the nonuniform spherical sampling ($\sin(\theta)$ is proportional to the sample area), and \mathcal{H} is a Huber loss.

3.2.1 Architecture

We now describe the structure of our cross-domain embedding model $f(y)$. With $f(y)$ we are predicting spatially dense spherical feature maps from a single 2D image. Convolutional encoder-decoder architectures with skip connections such as U-Net [27] or Stacked Hourglass [22] produce excellent results when some pixelwise association can be made between the input and output domains (e.g. for dense labeling tasks like semantic segmentation [2]). However, we must learn a cross-domain map from 2D image (Euclidean) to spherical functions. In this setting, architecture features such as skip connections are not only unnecessary but can be harmful by forcing the network to incorrectly consider associations across topologies.

We consider an encoder-decoder architecture, with several rounds of downsampling from input image to a 1D vector, followed by rounds of upsampling from the 1D vector to the set of spherical feature maps. We follow the best practices for this kind of architecture proposed by Radford *et al.* [25], employing a fully convolutional network with strided convolutions for downsampling and transposed convolutions for upsampling. We also found performance improvements by replacing convolutional layers with residual layers [12]. Figure 3 shows the architecture.

Given an input with dimensions $N \times N$, our best encoder was an architecture with $\log_2 N - 1$ blocks of 2 residual layers each. The number of channels double at each block, starting at 64 and capped at 256. The 1D encoding is upsampled using a sequence

of residual blocks up to the desired resolution. In our experiments, to predict spherical feature maps from single views, we render the views at a resolution of 128×128 , and use 1024 units in the 1D encoding.

3.2.2 Target embeddings

The remaining decision is to select the appropriate target feature maps from $s(x)$. For all our experiments $s(x)$ is a 10 layer residual spherical CNN trained for ModelNet40 3D shape classification on 64×64 inputs (i.e. $r(M)$ produces a single-channel 64×64 output). The decision of which feature maps to use as the target is application-dependent. For category-based relative pose estimation, we want features that are void of instance level details, which is achieved by taking the target embedding from deeper layers. Specifically we choose the 16×16 feature maps from $s(x)$. We employ the same target embedding for relative pose experiments on all datasets (ModelNet40, ObjectNet3D and ShapeNet), which shows some generalization. For view synthesis, we wish that the instance-level details are preserved, so we embed to an earlier layer, at resolution 32×32 .

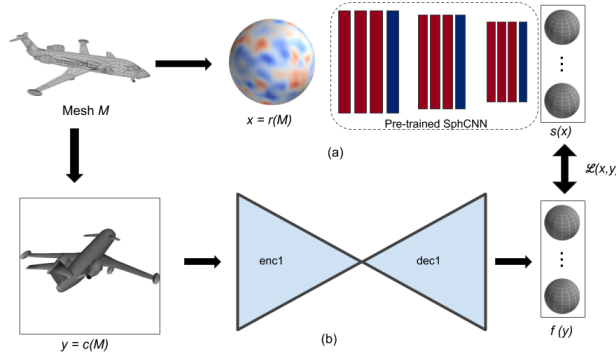


Figure 3: **Cross-domain spherical embeddings.** Given a 3D mesh, (a) we convert it to a spherical function, and use a pre-trained spherical CNN to compute its spherical embedding. (b) During training, we render a view and learn the transformation to the target spherical embedding using an encoder-decoder. During inference, the inputs are 2D images and only the encoder-decoder part is used.

3.2.3 Relative pose estimation

The cross-domain embeddings produced by $f(y)$ are sufficient to recover the relative pose between pairs of images (even between different instances of the same object category). As $f(y)$ produces spherical feature maps that have been trained to be 3D rotation equivariant, we can apply 3D rotations directly to the feature maps. Relative orientation estimation is simply identifying the rotation that brings feature maps into alignment. For alignment we use a very simple cross-correlation measure. Given two images y_1, y_2 we estimate their relative pose as

$$\arg \max_{R \in \mathbf{SO}(3)} G(R) = \sum_{k=0}^{K-1} \int_{p \in S^2} f(y_1)_k(p) \cdot f(y_2)_k(R^T p) dp \quad (7)$$

Here the subscript k denotes the k -th spherical channel in the image embedding. $G(R)$ can be evaluated efficiently in the spectral domain (similar in spirit to spherical convolution, see [18, 20] for details and implementation). The resolution of $G(R)$ depends on the resolution of the input spherical functions $f(y_1)$ and $f(y_2)$. Our learned feature maps have a spatial resolution of 16×16 which corresponds to a cell width of 22.5 deg at the equator, which we consider be too coarse for precise relative pose. To increase resolution, we upsample the features by a factor of 4 using bicubic interpolation prior to evaluating (7).

Recall, during training we take as input arbitrarily oriented meshes. A training example consists of only the target embeddings from the pretrained $s(r(M))$ and a single view rendered from a fixed camera $c(M)$. No orientation supervision is required, and the model never sees pairs of images together at training. This reduces the sample complexity and leads to faster convergence.

3.2.4 Novel view synthesis

The spherical embeddings learned by our method can also be applied towards novel view synthesis. The rotation equivariant spherical CNN feature maps undergo the same rotation as its inputs, so if we learn the inverse map that generates an image back from

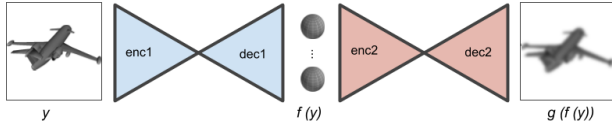


Figure 4: **Novel view synthesis training.** We learn the inverse map from spherical embeddings to 2D views. The map from 2D view to spherical embeddings (in blue) is the same as in Fig. 3 and is frozen during training. The synthesizer network (in red) reconstructs the same input view and is trained with an L_2 loss.

its embedding, we can rotate the embeddings and generate novel views.

We define the inverse map $g = f^{-1}$ such that $g(f(y)) = y$. If we let $y_1 = c(M)$ and $y_2 = c(\Lambda_R M)$ (i.e. $y_{1,2}$ are images of shape M before and after it undergoes a 3D rotation, respectively). It follows that

$$g(\Lambda_R f(y_1)) = g(f(y_2)) = y_2. \quad (8)$$

This gives us a way to generate a novel view of the 3D object under rotation, from the spherical embedding of a single view as follows (see Fig. 1 for illustration):

1. Obtain the embedding $f(y_1)$ of given view y_1 ,
2. Rotate the embedding by the desired $R \in \mathbf{SO}(3)$, obtaining $f(y_2) = \Lambda_R f(y_1)$,
3. Apply the inverse map g to obtain the novel view $y_2 = g(f(y_2))$.

Since g is learning the inverse of f , we similarly design g as a convolutional encoder-decoder, which is trained from single views enforcing $g(f(y)) = y$ with a pixel-wise L_2 loss $\mathcal{L}_s(y) = \|g(f(y)) - y\|_2^2$ (see Fig. 4 for illustration).

4 Experiments

4.1 Datasets

We utilize the standardized large datasets of 3D shapes ModelNet40 [40] and ShapeNet [1] for our experiments.

Some methods must explicitly deal with the symmetries present in many shape categories (e.g. [28, 24]). Our method is immune to this problem by not requiring pose annotations. However, pose annotations are used for evaluation, therefore we limit our experiments to categories which are largely free of symmetry and thus for which relative orientation is uniquely defined.

We utilize the following six categories from ModelNet40: *airplane*, *bed*, *car*, *chair*, *sofa*, and *toilet*, and the following from ShapeNet: *airplane*, *car*, *chair*, and *sofa*. Symmetry is a problem for the evaluation of ShapeNet *airplanes*. Some of the instances (e.g. spaceships and flying wings) are fully symmetric around one axis, which results in non-injective embeddings and two possible correct alignments that differ by 180 deg. For meaningful evaluation we compute the errors up to symmetry for this class.

Recall that we are not estimating pose relative to a canonical object frame but rather relative object orientation from a pair of images. Thus, for training, we do not require that our dataset models come aligned per category, and in fact we introduce random rotations at training time. For evaluation, in order to quantify our inter-instance performance we require aligned shapes to determine the ground truth (see Section 4.2); for ModelNet40 we use the aligned version from [29].

Multiple datasets have been proposed for object pose estimation, such as Pascal3D+ [42], KITTI [10], and Pix3D [31], but they do not exhibit large variation in viewpoints, especially camera elevation. For example Pascal3D+ has most elevations concentrated inside $[-10^\circ, 10^\circ]$ and the official evaluation only considers azimuthal accuracy. In our setting we explore geometric embeddings that can capture more challenging arbitrary viewpoints. Our results indicate that the problem of relative orientation from two views is quite difficult even for rendered images from ModelNet40 and ShapeNet. Our experiments with real images are limited to the *airplane* category of ObjectNet3D [41], which has the largest variety of viewpoints among categories in the dataset.

4.2 Relative pose estimation

For training, we render views in arbitrary poses sampled from $\mathbf{SO}(3)$. We have two modes of evaluation: *instance* and *category* based. For category-based, we measure the relative pose error between each instance and 3 randomly sampled instances from the test set. For instance-based, we measure the error between each instance from the test set and 3 randomly rotated versions of itself. The error is the angle between the estimated and ground truth relative poses; given input ground truth poses R_1 and R_2 and estimated pose R , it is given by $\arccos((\text{tr}(R_2^\top R_1 R) - 1)/2)$.

We compare with variations of a method based on [19], which treats pose estimation as a regression problem. To keep the comparison fair we use approximately the same number of parameters in the encoder as our networks, include their final layers to regress from the 1D bottleneck to pose, and use a combination of RMSE and geodesic pose loss as indicated. However, note that [19] requires the ground truth pose with respect to a canonical orientation during training, whereas our method is self-supervised and can operate on unaligned meshes. We still outperform their method even when allowing it the extra information, especially in the presence of 3DOF rotations. For completeness, we also include regression results to estimate error to a canonical pose. We also trained variants of this architecture to directly regress relative pose from pairs of images, however these architectures did not outperform a regression model to predict canonical pose.

On ShapeNet, we also compare with KeypointNet [33], which is an unsupervised method of learning keypoints that can be used for pose estimation. It makes the same assumptions about training data as our method: access to meshes from which we can render arbitrary views. The only difference is that while they assume 2DOF rotations, they only sample viewpoints on a hemisphere, whereas we sample the whole sphere. We retrain and evaluate KeypointNet with 3DOF rotations, but only the *chair* category converges. Our method also outperforms KeypointNet on the more challenging scenarios.

Table 1 shows the results for 3DOF alignment and Table 2 for 2DOF alignment for ModelNet40. Ta-

bles 3 and 4 show the same for ShapeNet.

Figure 5 shows a visualization of the 3DOF alignment quality on ShapeNet by rendering views using the estimated relative poses.

		airplane	bed	chair	car	sofa	toilet
IB	Regr.	11.8	26.0	43.7	16.5	25.3	17.8
	Ours	7.23	4.93	7.79	3.95	6.51	5.17
CB	Regr.	12.9	29.9	52.5	15.2	34.5	17.8
	Ours	8.81	8.55	15.3	5.12	11.0	10.9
C	Regr.	7.94	14.9	24.4	8.72	13.4	10.4

Table 1: Median angular error in degrees for instance (IB) and category-based (CB) 3DOF alignment on ModelNet40. ‘‘C Regression’’ refers to the problem of aligning to a canonical pose and is shown only for completeness.

		airplane	bed	chair	car	sofa	toilet
IB	Regr.	6.29	12.7	25.5	6.84	12.5	9.76
	Ours	3.33	4.46	7.07	4.12	4.52	4.88
CB	Regr.	7.13	15.8	32.2	7.00	13.3	10.4
	Ours	4.80	6.60	10.2	4.82	9.56	10.8
C	Regr.	4.55	7.46	14.3	4.52	7.07	6.10

Table 2: Median angular error in degrees for instance (IB) and category-based (CB) 2DOF alignment on ModelNet40.

4.2.1 Extension to real images

Most labeled real-world object pose estimation datasets have restricted pose variations. One dataset with sufficient variation of 3D poses is the aeroplane class in ObjectNet3D [41]. We assume object instance bounding boxes are provided (e.g. using an object detection network [8]). We train our model on image-mesh pairs and obtain a median relative angle error of **7.81** deg on test set image pairs, up to a 180 deg rotation due to symmetry, which in some cases cannot be captured by the low resolution spherical CNN feature maps (see bottom right of Figure 6 for an example). Figure 6 shows alignment results. The method based on regression achieves a significantly higher error of 35.2 degrees in the same task, also up to the 180 deg rotation.



Figure 5: **Category-based relative pose estimation.** We render one object in the pose of the other using our estimated relative pose. *For each block, top:* Inputs 1 and 2, from the test set. *Bottom:* Input 2 rotated into pose 1, and input 1 rotated into pose 2. We render from the ground truth meshes for visualization purposes only; the inputs to our method are solely the 2D views and the output is the relative pose. Note how the alignment is possible even under large appearance variation.

		airplane	chair	car	sofa
IB	Regression	43.8	19.9	9.54	20.5
	KeypointNet	div.	30.9	div.	-
	Ours	6.64	5.54	3.84	5.21
CB	Regression	44.5	24.7	10.7	24.4
	KeypointNet	div.	34.4	div.	-
	Ours	7.27	12.3	4.59	9.66
C	Regression	32.2	13.9	6.30	11.9

Table 3: Median angular error in degrees for instance (IB) and category-based (CB) 3DOF alignment on ShapeNet.

		airplane	chair	car	sofa
IB	Regression	16.8	13.7	6.55	17.0
	KeypointNet	5.72	5.42	3.37	-
	Ours	5.17	5.07	3.70	4.59
CB	Regression	20.3	17.1	7.22	19.7
	KeypointNet	18.6	14.3	11.8	-
	Ours	6.24	12.1	4.73	10.8
C	Regression	9.41	9.35	4.27	10.5

Table 4: Median angular error in degrees for instance (IB) and category-based (CB) 2DOF alignment on ShapeNet. Note that KeypointNet’s space of rotations is smaller than ours.

4.3 Novel view synthesis

We evaluate novel view synthesis qualitatively. Figure 7 shows the results for several generated views in different poses, with a single 2D image as input. We do not expect to generate realistic images here, since the embeddings do not capture color or texture and the generator is trained with an L_2 loss instead of perceptual or adversarial. Our goal is to demonstrate the learned embeddings naturally capture the geometry, which is demonstrated by this example, where a simple 3D rotation of the spherical embeddings obtained from a single 2D image produces a novel view

of the corresponding 3D object rotation. Adversarial and perceptual losses can be used in conjunction with our approach for refining the novel views [16, 37].

4.4 Discussion

Our image to spherical cross-domain embeddings show quantitative improvements over state-of-art in relative 3D object pose estimation. Most existing literature shows results on a restricted set of rotations, and our numbers on 2DOF rotations are comparable to state-of-art. However, for full 3DOF rotations,



Figure 6: **Relative pose estimation for real images.** We render the mesh corresponding to one input in the pose of the other using our estimated relative pose. *For each block, top:* Inputs 1 and 2, from the test set. *Bottom:* Mesh 2 rotated into pose 1, and mesh 1 rotated into pose 2. Image pairs on the top row map to the same mesh in the dataset; on the bottom they map to different meshes. The bottom-right block shows a typical failure case due to symmetry. Meshes are used for visualization purposes only; the inputs to our method are the 2D images and the relative pose is estimated directly from their embeddings via cross-correlation (see text for details).

relative pose estimation from 2D images is especially challenging for approaches which attempt to predict the pose directly from an image embedding, since it requires the network to see all possible rotations, and hence requiring a combinatorially large training dataset. In contrast, our approach learns the mapping using fewer viewpoints and the corresponding equivariant spherical embeddings.

For KeypointNet [33], training failed to converge for the car and airplane classes under challenging 3DOF rotations (noted ‘div’ in the table).

Evaluation of the *airplane* class is problematic on ShapeNet due to the presence of symmetric instances (flying wings and some spaceships), which admit two possible alignments that differ by an 180 deg rotation. We also observe problems on ObjectNet3D, but in this case it’s an approximate symmetry that is not captured by the low resolution spherical CNN feature maps. In both cases we consider the symmetry when evaluating the errors by making $\text{err}_{\text{sym}} = \min(\text{err}, \pi - \text{err})$. None of these problems are present in ModelNet40 *airplanes*.

Our method is capable of synthesizing any new viewpoint from any other given viewpoint for any instance of the class it was trained on. In figure 7 we only show one trajectory being generated from a canonical pose. The categories with less variation

(such as ModelNet40 airplanes) are easier to learn and produce sharper images. For all classes, however, we can verify that the full 3D information is captured by the embeddings.

5 Conclusion

In this paper, we explore the problem of learning expressive 3D rotation equivariant embeddings for 2D images. We proposed a novel cross-domain embedding that maps 2D images to spherical feature maps generated by spherical CNNs trained on 3D shape datasets. In this way, our cross-domain embeddings encode images with sufficient shape properties and an equivariant structure that together are directly useful for numerous tasks, including relative pose estimation and novel view synthesis.

There are two important properties of our model that we wish to highlight as areas for future work. First, the cross-domain embedding architecture is composed of a large encoder-decoder structure. The capacity of such a model is greater than what would be necessary for training traditional task-specific models (e.g. a relative pose regression network). This is due to the fact that we are solving a much harder problem: our model must learn a very expressive feature representation that can generalize to many appli-

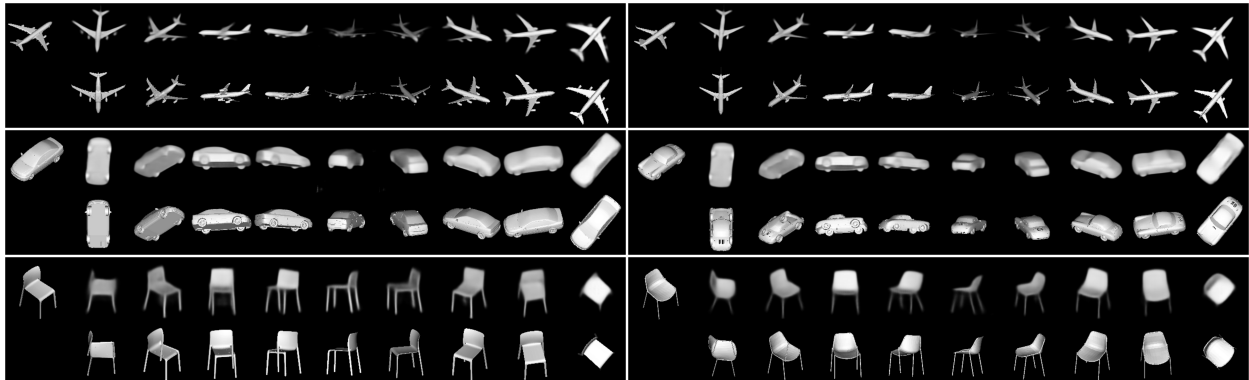


Figure 7: **Novel view synthesis.** *Top-left:* inputs, which are 2D images from the test set. *Top row:* novel views generated using our method. *Bottom row:* ground truth views rendered from the original mesh. Our embeddings are category based and capture both geometry and appearance, can be rotated as spheres, and can be inverted through another neural network.

cations. Nonetheless, in future work, we will explore ways to make this component more compact. Second, by construction, our work is tied to the spherical CNNs we use to supervise our embeddings. We will explore alternative rotation equivariant models supervise our training.

Going forward we will also try to improve our embedding representation so that they can be useful for even more challenging tasks such as textured view synthesis for example.

References

- [1] A. X. Chang, T. Funkhouser, L. Guibas, P. Hanrahan, Q. Huang, Z. Li, S. Savarese, M. Savva, S. Song, H. Su, J. Xiao, L. Yi, and F. Yu. ShapeNet: An Information-Rich 3D Model Repository. Technical Report arXiv:1512.03012 [cs.GR], Stanford University — Princeton University — Toyota Technological Institute at Chicago, 2015. 7
- [2] L.-C. Chen, Y. Zhu, G. Papandreou, F. Schroff, and H. Adam. Encoder-decoder with atrous separable convolution for semantic image segmentation. In *ECCV*, 2018. 5
- [3] T. S. Cohen, M. Geiger, J. Khler, and M. Welling. Spherical CNNs. In *International Conference on Learning Representations*, 2018. 1, 3, 4
- [4] T. S. Cohen and M. Welling. Group equivariant convolutional networks. 2016. 3
- [5] S. M. A. Eslami, D. Jimenez Rezende, F. Besse, F. Viola, A. S. Morcos, M. Garnelo, A. Ruderman, A. A. Rusu, I. Danihelka, K. Gregor, D. P. Reichert, L. Buesing, T. Weber, O. Vinyals, D. Rosenbaum, N. Rabinowitz, H. King, C. Hillier, M. Botvinick, D. Wierstra, K. Kavukcuoglu, and D. Hassabis. Neural scene representation and rendering. *Science*, 360(6394):1204–1210, 2018. 3
- [6] C. Esteves, C. Allen-Blanchette, A. Makadia, and K. Daniilidis. Learning SO(3) equivariant representations with spherical cnns. In *The European Conference on Computer Vision (ECCV)*, September 2018. 1, 3, 4
- [7] L. Falorsi, P. de Haan, T. R. Davidson, N. D. Cao, M. Weiler, P. Forr, and T. S. Cohen. Explorations in homeomorphic variational auto-encoding. *CoRR*, 2018. 3
- [8] A. Fathi, A. Korattikara, C. Sun, I. Fischer, J. Huang, K. Murphy, M. Zhu, S. Guadarrama, V. Rathod, Y. Song, and Z. Wojna. Speed and accuracy trade-offs for modern convolutional object detectors. Honolulu, Hawaii, 2017. 8
- [9] J. Flynn, I. Neulander, J. Philbin, and N. Snavely. Deepstereo: Learning to predict new views from the world’s imagery. In *The IEEE Conference on Computer Vision and Pattern Recognition (CVPR)*, 2016. 3

- [10] A. Geiger, P. Lenz, and R. Urtasun. Are we ready for autonomous driving? the KITTI vision benchmark suite. In *IEEE Conference on Computer Vision and Pattern Recognition (CVPR)*, 2012. 7
- [11] A. Grabner, P. M. Roth, and V. Lepetit. 3d pose estimation and 3d model retrieval for objects in the wild. *CoRR*, 2018. 3
- [12] K. He, X. Zhang, S. Ren, and J. Sun. Identity mappings in deep residual networks. *CoRR*, abs/1603.05027, 2016. 1, 5
- [13] P. Henderson and V. Ferrari. Learning to generate and reconstruct 3d meshes with only 2d supervision, 2018. 3
- [14] M. Jaderberg, K. Simonyan, A. Zisserman, and k. kavukcuoglu. Spatial transformer networks. In *NIPS*, pages 2017–2025. 2015. 2
- [15] A. Kanazaki, Y. Matsushita, and Y. Nishida. Rotationnet: Joint object categorization and pose estimation using multiviews from unsupervised viewpoints. In *IEEE International Conference on Computer Vision and Pattern Recognition*, 2018. 3
- [16] T. Karras, T. Aila, S. Laine, and J. Lehtinen. Progressive growing of GANs for improved quality, stability, and variation. In *International Conference on Learning Representations*, 2018. 9
- [17] R. Kondor and S. Trivedi. On the generalization of equivariance and convolution in neural networks to the action of compact groups. In *International Conference on Machine Learning, ICML*, 2018. 3
- [18] P. J. Kostelec and D. N. Rockmore. Ffts on the rotation group. *Journal of Fourier analysis and applications*, 14(2):145–179, 2008. 6
- [19] S. Mahendran, H. Ali, and R. Vidal. 3d pose regression using convolutional neural networks. In *IEEE Conference on Computer Vision and Pattern Recognition Workshops (CVPRW)*, 2017. 3, 8
- [20] A. Makadia and K. Daniilidis. Spherical correlation of visual representations for 3d model retrieval. *International Journal of Computer Vision*, 89(2):193–210, 2010. 6
- [21] A. Mousavian, D. Anguelov, J. Flynn, and J. Kosecka. 3d bounding box estimation using deep learning and geometry. In *CVPR*, 2017. 3
- [22] A. Newell, K. Yang, and J. Deng. Stacked hourglass networks for human pose estimation. In *European Conference on Computer Vision*, pages 483–499. Springer, 2016. 5
- [23] G. Pavlakos, X. Zhou, A. Chan, K. G. Derpanis, and K. Daniilidis. 6-DoF object pose from semantic keypoints. In *International Conference on Robotics and Automation (ICRA)*, 2017. 3
- [24] M. Rad and V. Lepetit. BB8: A scalable, accurate, robust to partial occlusion method for predicting the 3d poses of challenging objects without using depth. In *IEEE International Conference on Computer Vision (ICCV)*, 2017. 7
- [25] A. Radford, L. Metz, and S. Chintala. Unsupervised representation learning with deep convolutional generative adversarial networks. *CoRR*, abs/1511.06434, 2015. 5
- [26] H. Rhodin, M. Salzmann, and P. Fua. Unsupervised geometry-aware representation for 3d human pose estimation. In *The European Conference on Computer Vision (ECCV)*, September 2018. 1, 3
- [27] O. Ronneberger, P. Fischer, and T. Brox. U-net: Convolutional networks for biomedical image segmentation. In *MICCAI*, 2015. 5
- [28] A. Saxena, J. Driemeyer, and A. Y. Ng. Learning 3-d object orientation from images. In *IEEE International Conference on Robotics and Automation*, 2009. 7
- [29] N. Sedaghat and T. Brox. Unsupervised generation of a viewpoint annotated car dataset from videos. In *IEEE International Conference on Computer Vision (ICCV)*, 2015. 7
- [30] H. Su, C. R. Qi, Y. Li, and L. J. Guibas. Render for cnn: Viewpoint estimation in images using cnns trained with rendered 3d model views. In *The IEEE International Conference on Computer Vision (ICCV)*, December 2015. 3
- [31] X. Sun, J. Wu, X. Zhang, Z. Zhang, C. Zhang, T. Xue, J. B. Tenenbaum, and W. T. Freeman. Pix3d: Dataset and methods for single-image 3d shape modeling. In *IEEE Conference on Computer Vision and Pattern Recognition (CVPR)*, 2018. 7
- [32] M. Sundermeyer, Z.-C. Marton, M. Durner, M. Brucker, and R. Triebel. Implicit 3d orientation learning for 6d object detection from rgb images. In *The European Conference on Computer Vision (ECCV)*, September 2018. 3
- [33] S. Suwajanakorn, N. Snavely, J. Tompson, and M. Norouzi. Discovery of latent 3d keypoints via end-to-end geometric reasoning. *arXiv preprint arXiv:1807.03146*, 2018. 3, 8, 10
- [34] M. Tatarchenko, A. Dosovitskiy, and T. Brox. Multi-view 3d models from single images with a convolutional network. *Lecture Notes in Computer Science*, page 322337, 2016. 3

- [35] S. Tulsiani and J. Malik. Viewpoints and key-points. In *Computer Vision and Pattern Recognition (CVPR)*, 2015. 3
- [36] S. Tulsiani, T. Zhou, A. A. Efros, and J. Malik. Multi-view supervision for single-view reconstruction via differentiable ray consistency. In *Computer Vision and Pattern Recognition (CVPR)*, 2017. 4
- [37] T.-C. Wang, M.-Y. Liu, J.-Y. Zhu, A. Tao, J. Kautz, and B. Catanzaro. High-resolution image synthesis and semantic manipulation with conditional gans. In *CVPR*, 2018. 9
- [38] D. E. Worrall, S. J. Garbin, D. Turmukhambetov, and G. J. Brostow. Harmonic networks: Deep translation and rotation equivariance. In *Proc. IEEE Conf. on Computer Vision and Pattern Recognition (CVPR)*, volume 2, 2017. 1, 3
- [39] D. E. Worrall, S. J. Garbin, D. Turmukhambetov, and G. J. Brostow. Interpretable transformations with encoder-decoder networks. In *The IEEE International Conference on Computer Vision (ICCV)*, volume 4, 2017. 3
- [40] Z. Wu, S. Song, A. Khosla, F. Yu, L. Zhang, X. Tang, and J. Xiao. 3d shapenets: A deep representation for volumetric shapes. In *IEEE Conference on Computer Vision and Pattern Recognition, CVPR*, 2015. 7
- [41] Y. Xiang, W. Kim, W. Chen, J. Ji, C. Choy, H. Su, R. Mottaghi, L. Guibas, and S. Savarese. Objectnet3d: A large scale database for 3d object recognition. In *European Conference Computer Vision (ECCV)*, 2016. 7, 8
- [42] Y. Xiang, R. Mottaghi, and S. Savarese. Beyond pascal: A benchmark for 3d object detection in the wild. In *IEEE Winter Conference on Applications of Computer Vision (WACV)*, 2014. 7
- [43] X. Yan, J. Yang, E. Yumer, Y. Guo, and H. Lee. Perspective transformer nets: Learning single-view 3d object reconstruction without 3d supervision. In *NIPS*. 2016. 1
- [44] J. Yang, S. E. Reed, M.-H. Yang, and H. Lee. Weakly-supervised disentangling with recurrent transformations for 3d view synthesis. In C. Cortes, N. D. Lawrence, D. D. Lee, M. Sugiyama, and R. Garnett, editors, *Advances in Neural Information Processing Systems 28*, pages 1099–1107. Curran Associates, Inc., 2015. 3
- [45] S. Yao, T. M. H. Hsu, J.-Y. Zhu, J. Wu, A. Torralba, B. Freeman, and J. Tenenbaum. 3d-aware scene manipulation via inverse graphics. *arXiv preprint arXiv:1808.09351*, 2018. 3
- [46] T. Zhou, S. Tulsiani, W. Sun, J. Malik, and A. A. Efros. View synthesis by appearance flow. In *European Conference on Computer Vision*, 2016. 3
- [47] Y. Zou, Z. Luo, and J.-B. Huang. Df-net: Unsupervised joint learning of depth and flow using cross-task consistency. In *European Conference on Computer Vision*, 2018. 1